

X-ray Emission Properties of Large Scale Jets, Hotspots and Lobes in Active Galactic Nuclei

Jun Kataoka¹ and Łukasz Stawarz²

¹*Tokyo Institute of Technology, Meguro, Tokyo, Japan*

²*Obserwatorium Astronomiczne, Uniwersytet Jagielloński, Kraków, Poland*

ABSTRACT

We examine a systematic comparison of jet-knots, hotspots and radio lobes recently observed with *Chandra* and *ASCA*. This report will discuss the origin of their X-ray emissions and investigate the dynamics of the jets. The data was compiled at well sampled radio (5 GHz) and X-ray frequencies (1keV) for more than 40 radio galaxies. We examined three models for the X-ray production: synchrotron (SYN), synchrotron self-Compton (SSC) and external Compton on CMB photons (EC). For the SYN sources — mostly jet-knots in nearby low-luminosity radio galaxies — X-ray photons are produced by ultrarelativistic electrons with energies 10–100 TeV that must be accelerated in situ. For the other objects, conservatively classified as SSC or EC sources, a simple formulation of calculating the “expected” X-ray fluxes under an equipartition hypothesis is presented. We confirmed that the observed X-ray fluxes are close to the expected ones for non-relativistic emitting plasma velocities in the case of radio lobes and majority of hotspots, whereas considerable fraction of jet-knots is too bright at X-rays to be explained in this way. We examined two possibilities to account for the discrepancy in a framework of the inverse-Compton model: (1) magnetic field is much smaller than the equipartition value, and (2) the jets are highly relativistic on kpc/Mpc scales. We concluded, that if the inverse-Compton model is the case, the X-ray bright jet-knots are most likely far from the minimum-power condition. We also briefly discuss the other possibility, namely that the observed X-ray emission from all of the jet-knots is synchrotron in origin.

Subject headings: galaxies: jets — magnetic fields — radiation mechanism: non-thermal

1. Introduction

The excellent spatial resolution of *Chandra* X-ray Observatory has opened a new era to study the large scale jets in powerful extragalactic radio sources. At the time of this writing, more than 40 radio-loud AGNs are known to possess X-ray counterparts of radio jets on kpc to Mpc scales (Harris & Krawczynski 2002, Stawarz 2004 and references therein; see also <http://hea-www.harvard.edu/XJET/>). Bright X-ray knots (hereafter “jet-knots”) are most often detected, but the X-ray emissions from the hotspots and radio lobes are also reported in a

number of FR II radio galaxies and quasars (e.g., Wilson, Young & Shopbell 2000; 2001; Hardcastle et al. 2002b; 2004, Tashiro et al. 1998; Isobe 2002).

The broad-band spectra of jet-knots, hotspots, and lobes detected by *Chandra* show great variety between radio and X-ray energy bands. In nearby FR I sources, typical X-ray-optical-radio spectrum of the jet-knots is consistent with a single smoothly broken power-law continuum, suggesting that this broad-band emission is entirely due to non-thermal synchrotron radiation from a single electron population (e.g., Marshall et al. 2002 and Wilson & Yang 2002 for M 87). In most other sources, however, the X-ray knots’ spectra are much harder than expected from a simple ex-

¹e-mail:kataoka@hp.phys.titech.ac.jp

²e-mail:stawarz@oa.uj.edu.pl

trapolation of the radio-to-optical fluxes. These situations are believed that both the radio and optical emissions are due to synchrotron radiation, whereas X-ray photons are produced via the inverse-Compton scattering of either synchrotron photons (SSC) or cosmic microwave background photons (EC; Tavecchio et al. 2000, Celotti, Ghisellini & Chiaberge 2001). Other (synchrotron) models have been also proposed to explain intense X-ray emission of the large-scale quasar jets (e.g., Dermer & Atoyan 2002, Stawarz & Ostrowski 2002). In the case of the hotspots in powerful sources one finds an analogous controversy regarding the X-ray emission: although in many objects this emission is consistent with the standard SSC model (see, e.g., Wilson et al. 2000 for Cygnus A), in some other sources it cannot be simply explained in this way, suggesting most likely a synchrotron origin of the detected X-ray photons (see, e.g., Hardcastle et al. 2004). For the extended lobes of quasars and FR IIs the X-ray radiation is established to be produced by the EC process involving CMB target radiation. In some cases, however, infrared target photons from quasar cores may contribute to the inverse-Compton lobes' emission at keV photon energy range (Brunetti, Setti & Comastri 1997).

In the standard picture of FR II radio galaxies and quasars, the relativistic jet is decelerated in a hotspot converting part of its energy into relativistic electrons and part in magnetic field. Then the shocked plasma moves inside the head region just behind the hotspot, and expands almost adiabatically to form diffuse, extended radio lobes. Even though this picture appears to be simple, much of the fundamental physics behind it remains unclear (see, e.g., recent monograph by De Young 2002a). For example, the velocity and dynamics of the large-scale jets is unknown. From the analogy to sub-pc jets in blazar-type AGNs, it is plausible that some of the FR II and quasar jets are highly relativistic even on kpc/Mpc scales. Recent studies on the optical emission of the large-scale jets seem to justify this hypothesis (e.g., Sparks et al. 1995, Scarpa & Urry 2002, Jester 2003), and the usually discussed versions of the EC model for the X-ray jet-knots indeed require the jet bulk Lorentz factors $\Gamma_{\text{BLK}} \geq 10$ (e.g., Harris & Krawczynski 2002). Yet, the exact velocity structure both along and across large-scale jets in

FR II radio galaxies and quasars remains an open issue. The strong terminal shocks at the hotspots are unlikely to be moving with high bulk Lorentz factors, but moderately relativistic motions ($\Gamma_{\text{BLK}} \leq \text{a few}$) are permitted by hydrodynamic simulations (e.g., Aloy et al. 1999). We note, that such simulations repeatedly reveal a complex hotspots' morphology, especially at the late stages of the jet evolution (e.g., Marti et al. 1997, Mizuta, Yamada & Takabe 2004). Finally, the main-axis expansion of radio lobe is thought to be sub-relativistic; $\Gamma_{\text{BLK}} \simeq 1$. However, detailed transport and spatial distribution of the radiating particles within the lobes of powerful radio sources is still being debated (e.g., Blundell & Rawlings 2000, Kaiser 2000, Manolakou & Kirk 2003).

As for the velocity of jet plasma, the strength of magnetic field in radio galaxies is an open matter. Assuming an equipartition field value in the lobes ($1-10 \mu\text{G}$), which seems to be supported by the X-ray lobes' observations, a simple flux conservation argument predicts the magnetic field in the jets as high as $0.01-1 \text{ G}$ (De Young 2002b). Such a strong magnetic field is problematic, since numerical simulations of Poynting-flux dominated jets (e.g., Komissarov 1999) cannot correctly reproduce the observed large-scale morphologies of powerful radio sources. Thus, an amplification of the magnetic field to the equipartition value in strong jet terminal shock and in its turbulent downstream region is required, although only little theoretical investigations of this issue has been reported (see De Young 2002b). Let us mention in this context, that turbulent processes that may lead to amplification of the magnetic field can manifest in formation of the flat-spectrum synchrotron X-ray features, such like the ones discovered recently in the hotspots of Cygnus A radio galaxy (Bałucińska-Church et al. 2004). On the other hand, the equipartition of energy between the magnetic field and the radiating electrons, established for some high-luminosity sources, may not be valid in general, especially in the case of low-luminosity hotspots (Hardcastle et al. 2004). Finally, we note that the configuration of the magnetic field within the lobes is also not well understood (see a discussion in Blundell & Rawlings 2000).

Unfortunately, present radio-to-X-ray observations are not sufficient to discriminate conclusively

between different models proposed in order to explain multiwavelength emission of the large-scale structures of powerful radio sources, and of their kpc/Mpc jets in particular. However, we believe that a systematic comparison between broad-band radiative properties of the jet-knots, hotspots, and lobes will provide important clues to dynamics and the physics of large scale jets, and to put some constraints on the models discussed in the literature. Keeping these motivations in mind, the purpose of this paper is to obtain a rough, but unified picture which may link the jet-knots, hotspots and radio lobes, rather than modeling individual sources in a sufficiently detailed manner. Obviously, detailed studies on individual cases are irreplaceable. In fact, many controversial issues briefly touched in this analysis will remain open until such detailed investigations, based on long multiwavelength observations, are performed. We emphasize, that our analysis confirms many results known from the literature (see, e.g., Stawarz 2004 for a review), although for a large number of sources modeled in addition in a uniform way. Basing on this homogeneous approach, we explore however some new, hardly discuss in the literature aspects of the physics behind the X-ray emission models for the considered objects. Let us also mention, that in this paper we do not consider hadronic models for the broad-band emission of the large-scale jets and their hotspots (see, e.g., Aharonian 2002, Atoyan & Dermer 2004).

Our presented study is based on data analysis for a sample consisting of 26 radio galaxies, 14 quasars, and 4 blazars. We collected all existing data at well sampled radio (5 GHz) and X-ray (1 keV) frequencies and analyzed them in a systematic manner. In §2, we defined sample selection and observables used in this paper. In §3, we presented a simple formulation of calculating the “expected” X-ray flux densities for the SSC and EC models taking the relativistic beaming effect into account. We then compared the physical quantities (beaming factor and the magnetic field) of the jet-knots, hotspots, and lobes. In §4 we discuss the results and the summary is presented in §5.

2. Data and analysis

2.1. Sample

Table 1 compiles a list of “X-ray jet sources” in which jet-knots, hotspots and/or radio lobes are detected by *Chandra* and *ASCA*. The first pioneer work have been reported by Harris & Krawczynski (2002), where the emission mechanisms of 18 X-ray jet sources (mainly jet-knots) are discussed in the framework of relativistically moving jet model. They continue to maintain current information at <http://hea-www.harvard.edu/XJET/>, which conveniently summarize the name, coordinate, distance, and morphology of the X-ray jet sources. Our sample contains all of the sources listed in this page, with additional information on the X-ray observations of radio lobes mainly organized by *ASCA*.

Before compiling the data, we have performed quick re-analysis of *Chandra* data (if already archived) to check the published results, and found no discrepancy. We therefore refer to published results (fluxes and spectral indices) unless otherwise stated in this paper. This gives a large number of objects known to us as of 2004 June, which contains 44 X-ray jet sources (56 jet-knots, 24 hotspots, and 18 radio lobes: see Table 2). We are aware that our sample is still incomplete, as the known X-ray jet sources are increasing their number day by day. Nevertheless such a list provides a convenient overview of X-ray jet sources detected so far, and provide a useful hint to *predict* fluxes of unobserved X-ray jet sources. We also note that Hardcastle et al. (2004) recently summarizes the X-ray emission properties of the hotspots in FR II radio galaxies.

The basic information about each source are listed in Table 1: (1) source name, (2) redshift z , (3) luminosity distance to the source d_L adopting $H_0 = 75 \text{ km s}^{-1} \text{ Mpc}^{-1}$ and $q_0 = 0.5$, (4) classification, and (5) references. RG denotes radio galaxy of either Fanaroff & Riley type I (FR I) or type II (FR II), QSO denotes either core dominated (CD) quasars or lobe dominated (LD) quasars, and BLZR denotes blazar-class.

More detailed information on each source are listed in Table 2. In the second column we denote “knot (K)” to indicate a distinct structure in the jet, “hotspots (HS)” as a terminal bright enhance-

ment at an end of the FR II jet or as one of the multiple features associated with a termination of the jet, and “lobe (L)” as a diffuse extended structure associated with a radio lobe. A suffix after K, HS, and L means the identification of each structure. For example “K-A” denotes ‘knot-A’ and “HS-SE” means “South-east hotspot”. In succeeding columns of Table 2, we have listed 6 observables: (1) α_R : radio spectral index measured at 5 GHz, (2) f_R : radio flux density at 5 GHz in mJy, (3) α_X : X-ray spectral index at 1 keV, (4) f_X : X-ray flux density at 1 keV in nJy, (5) f_O : optical flux density at 5×10^{14} Hz in μ Jy, and (6) θ : radial size of the emitting region in arcsec. When observations have not been reported at 5 GHz or 1 keV, we calculate the flux by extrapolating the nearest measured frequency by assuming the spectral index listed in the table. A suffix f means that we have assumed the fixed value for this calculation.

2.2. Radio/X-ray comparison

Figure 1 shows the distribution of the spectral indices in the radio band (α_R ; *upper*) and in the X-ray band (α_X ; *lower*), respectively. Note that radio spectral index shows a relatively narrow distribution centered at 0.8 and there is no clear difference between the jet-knots, hotspots and radio lobes. As is widely believed, the radio emissions of these sources are most likely due to the synchrotron radiation from the low-energy population of relativistic electrons. In other words, energy index of accelerated electron is narrowly distributed around $s = (\alpha_R + 1)/2 \simeq 2.6$, which is slightly steeper than the one expected from a diffusive acceleration at nonrelativistic shocks, $s = 2$. Let us note in this context, that analytical and numerical studies of particle acceleration at relativistic shocks (reviewed by, e.g., Kirk & Duffy 1999 and Ostrowski 2002), indicate that in such a case one can expect variety of particle spectra, with the asymptotic power-law inclination $s = 2.2$ for the strong turbulence condition and ultrarelativistic shock velocity. We also note, that stochastic second-order Fermi processes do not favor any universal value of the power-law spectral index characterizing accelerated electrons.

Meanwhile, the X-ray energy index, α_X , is widely distributed from 0.2 to 1.6. Part of the reason may be relatively large uncertainties in determining the spectral shape of faint X-ray sources

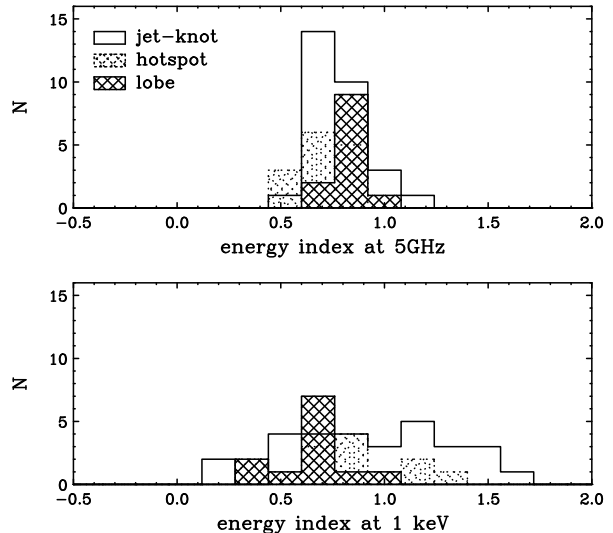


Fig. 1.— Distribution of the energy index measured at 5 GHz and at 1 keV.

compared to the radio spectral shape, but even if only bright (i.e., small error bars) X-ray sources are plotted, the same trend is obtained. Steep X-ray sources are most frequently found in nearby FR I radio galaxies. As discussed in the literature, the X-ray fluxes in these sources may smoothly connect with radio/optical fluxes and hence are considered to be the highest energy tail of the synchrotron radiation. For the X-ray emission from other jet-knots the situation is less clear. Flat X-ray spectral indices may indicate pile-up effects at the high-energy part of the electron energy distribution, advocating thus synchrotron origin of the keV photons (see Harris, Mossman & Walker 2004), or, oppositely, spectral flattenings occurring at the low-energy part of the electron continuum thus being consistent with the EC interpretation of the X-ray knots’ emission. Clearly, spectral information alone are not sufficient at the moment to distinguish either between synchrotron and inverse-Compton origin of the keV photons from the jet-knots in most of the cases, or to indicate the appropriate particle acceleration process.

Figure 2 presents the distribution of luminosity ratio of L_R and L_X , where $L_R = 4\pi d_L^2 f_R \nu_R$ and $L_X = 4\pi d_L^2 f_X \nu_X$, respectively. Note that a clear difference can be seen between the jet-knot and hotspot or radio lobes. The jet-knots tend to be much brighter in X-rays compared to the hotspots

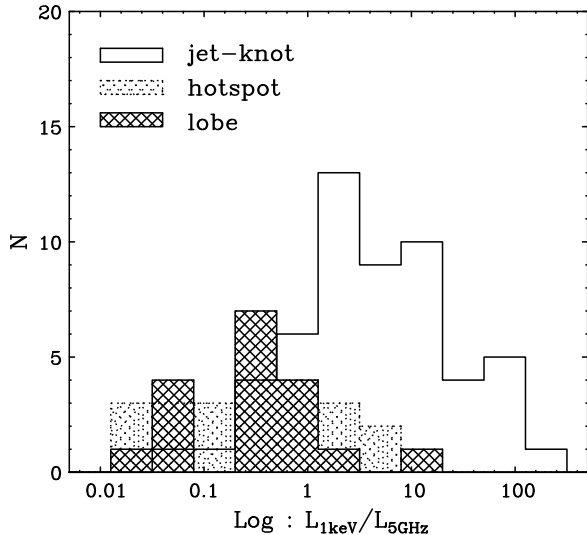


Fig. 2.— Distribution of the ratio between $L_{1\text{keV}}$ and $L_{5\text{GHz}}$.

and radio lobes. This trend is seen more clearly in Figure 3, where the correlation between L_R and L_X is plotted in two dimensional space. One finds several important tendencies which cannot be accounted by the sampling bias effect. First, hotspots and radio lobes occupy only the high-luminosity part of the plot, namely $\geq 10^{40}$ erg s^{-1} . Secondly, low-luminosity hotspots tend to be brighter in X-ray, as has been pointed out by Hardcastle et al. (2004). Thirdly, $L_R \geq L_X$ for most of the hotspots and radio lobes, but most of the jet-knots show an opposite trend.

We should note that due to limited sensitivity of *Chandra* (typically 0.1 nJy at 1 keV for 10 ksec exposure), we would not expect to detect the X-ray emission from the “X-ray faint” jet-knots. Therefore the lack of the X-ray faint (i.e., $L_R \geq L_X$) jet-knots at the bottom left corner of Figure 3 would be biased by the sensitivity of *Chandra* detector. In fact, we can find a few X-ray faint jet-knots at the top right corner, where the luminosity is the highest. However, even if only high-luminosity sources are selected, we can see a clear difference between the jet-knots, hotspots and radio lobes, namely “X-ray bright” sources are found only in jet-knots. Apparently, this is not due to the sampling effect since we certainly would have been able to detect “X-ray bright” hotspots if they existed.

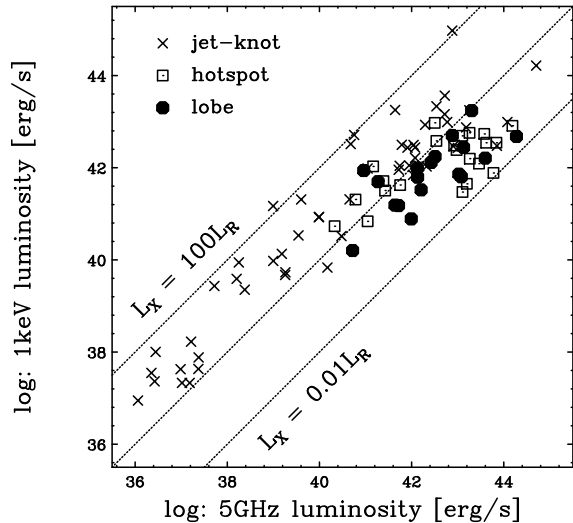


Fig. 3.— Relation between the luminosities $L_{5\text{GHz}}$ and $L_{1\text{keV}}$.

3. Model application to data

In this section we present a simple formulation of computing an equipartition magnetic field strength B_{eq} from an observed radio flux f_R measured at a radio frequency ν_R . Next, we calculate the “expected” SSC and EC luminosities for B_{eq} , to compare them with the observed X-ray luminosities. In the analysis, we include possible relativistic bulk velocity of the jet plasma. Taking the obtained results into account, and analyzing additionally the observed broad-band spectral properties of the compiled sources (including optical fluxes), we follow the “conservative” classification of the compiled X-ray sources into three groups, namely (i) synchrotron involving single/broken power-law electron energy distribution (SYN), (ii) synchrotron self-Compton (SSC) and (iii) external Compton of CMB photons (EC). Finally, we discuss the validity of the applied classification scheme, and compare it briefly with the classification introduced in the literature.

3.1. Equipartition magnetic field

In order to determine the X-ray emission properties of the large-scale jets, we first estimated the magnetic field strength under the minimum-power hypothesis using the observed radio luminosities

measured at 5 GHz. As we have reviewed in §1, it is generally believed that the magnetic field energy density u_B and the particle energy density u_e may be close to the equipartition in a number of radio sources. Therefore our approach is that we first assume an equipartition to calculate “predicted” inverse-Compton X-ray luminosities, and then compare them to the observed ones. If a large discrepancy occurs, this may suggest that equipartition is strongly violated, that the inverse-Compton origin of the observed keV photons is not the case, or that we have to consider another correction factor, such as Doppler beaming factor δ , as we will discuss below.

Since the synchrotron luminosity, L_ν , is proportional to $u_e u_B V$, where V is the volume of the emitting regions, we can estimate the equipartition magnetic field B_{eq} for a given luminosity observed at a radio frequency ν . Under the assumption of *no* relativistic beaming ($\delta = 1$), B_{eq} is expressed as

$$B_{\text{eq}, \delta=1} = \left[\frac{3\mu_0 G(\alpha)\eta L_\nu}{2V} \right]^{2/7} \propto \left(\frac{\eta L_\nu}{V} \right)^{2/7} \nu^{1/7}, \quad (1)$$

where μ_0 is permeability of free space, $G(\alpha)$ is a function given in Longair (1994), α is the spectral energy index and L_ν is the synchrotron luminosity measured at a frequency ν . η is the ratio of energy density carried by proton and electrons to the energy density of the electrons, i.e., $\eta = 1$ for the leptonic (e^-e^+) jet and $\eta = 1836$ for the hadronic (e^-p^+) jet for which the ratio of proton to electron energy densities equals the ratio of their rest masses. In the last approximation in the equation (1) we put minimum synchrotron frequency $\nu_{\text{min}} = \nu$ and $\alpha = 0.75$. The latter choice is justified by a narrow distribution of the radio spectral indices in the compiled dataset (Figure 1, *upper*). The former choice gives the *minimum* value of B_{eq} for the observed L_ν at some given frequency ν . Below we consider $\nu = \nu_R = 5$ GHz, although it is obvious that the minimum radio frequency has to be lower than this (especially in the case of the EC model, which requires presence of low-energy electrons with energies below GeV). However, the difference between equipartition magnetic field computed for $\nu_{\text{min}} = \nu$ and for $\nu_{\text{min}} \neq \nu$, respectively, is

rather small, $\propto (\nu_{\text{min}}/\nu)^{1/14}$. In addition, the expected spectral flattenings at the low-energy part of the synchrotron continuum are likely to make this difference even smaller.

In general, an emission volume, V , is quite uncertain for astrophysical sources due to the limited angular resolution of detectors and projection effect. We have assumed that the emitting region has a spherical volume of a certain angular radius θ ["] for all the jet structures. This is obviously an over-simplified assumption, however it significantly reduces the complexity of the models. Most of the jet-knots and hotspots are point-like sources when observed with *Chandra*. We therefore set an upper limit of $\theta = 0.3''$, unless there are additional radio/optical observations obtained with better angular resolution. Meanwhile a number of radio lobes show extended structures, but morphology is more complicated than a homogeneous sphere. We therefore calculated the volume by assuming a cylinder or a rotational ellipse, and then approximated it as a sphere which has an equal volume.

For a relativistically moving plasma, the equipartition magnetic field measured in the emitting plasma rest frame is related to the equipartition value computed for no beaming by the relation (Stawarz, Sikora & Ostrowski 2003)

$$B_{\text{eq}} = B_{\text{eq}, \delta=1} \delta^{-5/7}. \quad (2)$$

The above expression can be more conveniently written as

$$B_{\text{eq}} = 123 \eta^{2/7} (1+z)^{11/7} \left(\frac{d_L}{100 \text{Mpc}} \right)^{-2/7} \times \left(\frac{\nu_R}{5 \text{GHz}} \right)^{1/7} \left(\frac{f_R}{100 \text{mJy}} \right)^{2/7} \left(\frac{\theta}{0.3''} \right)^{-6/7} \times \delta^{-5/7} [\mu\text{G}], \quad (3)$$

where d_L is the luminosity distance to the source, and f_R is the observed radio luminosity measured at frequency ν_R . $B_{\text{eq}, \delta=1}$ for various jet sources are calculated in Table 2 for $\eta = 1$, what gives again the *minimum* value of $B_{\text{eq}, \delta=1}$. We note that this particular choice does not refer exclusively to the leptonic jet model. For example, it may refer to the case of energy equipartition between jet magnetic field and radiating electrons

solely. We note, that the discussion on the jet composition is still open, and the situation may be quite complex as, for example, the jet can be composed predominantly from the e^-e^+ -pairs, but still remain dynamically dominated by the (cold) hadrons (see Sikora & Madejski 2000).

3.2. Synchrotron (SYN) case

We first consider the case where the X-ray emissions are due to the synchrotron radiation emitted by the electrons with the Lorentz factor γ_X . We assume that the magnetic field in the jet moving plasma is close to equipartition B_{eq} , and its relativistic beaming factor is δ . Then the observed X-ray frequency is given by

$$\begin{aligned}\nu_X &\simeq 1.2 \times 10^6 \gamma_X^2 B_{\text{eq}} (1+z)^{-1} \delta \\ &\simeq 1.2 \times 10^6 \gamma_X^2 B_{\text{eq}, \delta=1} (1+z)^{-1} \delta^{2/7}.\end{aligned}\quad (4)$$

The respective electron Lorentz factor, γ_X , is hence given as

$$\begin{aligned}\gamma_X &\simeq 4.5 \times 10^7 \left(\frac{\nu_X}{\nu_{1\text{keV}}} \right)^{1/2} \left(\frac{B_{\text{eq}, \delta=1}}{100 \mu\text{G}} \right)^{-1/2} \\ &\quad \times (1+z)^{1/2} \delta^{-1/7},\end{aligned}\quad (5)$$

where $\nu_{1\text{keV}}$ is 2.4×10^{17} Hz. Therefore, even though δ is quite uncertain, the estimated value of γ_X is not affected significantly since γ is only weakly dependent on δ , i.e., $\propto \delta^{-1/7}$.

3.3. Synchrotron self-Compton (SSC) emission

The observed radio frequency is approximately

$$\nu_R \simeq 1.2 \times 10^6 B_{\text{eq}} \gamma_R^2 (1+z)^{-1} \delta, \quad (6)$$

where γ_R is a Lorentz factor of electrons which emit synchrotron photons at ν_R . In the SSC case, electrons upscatter synchrotron photons to a frequency

$$\begin{aligned}\nu_{\text{IC}} &\simeq \frac{4}{3} \gamma_R^2 \nu_R = 2.8 \times 10^{17} \left(\frac{\nu_R}{5\text{GHz}} \right)^2 \left(\frac{B_{\text{eq}}}{100 \mu\text{G}} \right)^{-1} \\ &\quad \times (1+z) \delta^{-1} \quad [\text{Hz}] \\ &= 2.3 \times 10^{17} \eta^{-2/7} (1+z)^{-4/7} \left(\frac{d_L}{100\text{Mpc}} \right)^{2/7} \\ &\quad \times \left(\frac{\nu_R}{5\text{GHz}} \right)^{13/7} \left(\frac{f_R}{100\text{mJy}} \right)^{-2/7} \left(\frac{\theta}{0.3''} \right)^{6/7} \\ &\quad \times \delta^{-2/7} \quad [\text{Hz}].\end{aligned}\quad (7)$$

Note that, ν_{IC} depends both on the observed radio frequency and magnetic field strength B_{eq} . To calculate the X-ray flux at an observed frequency ν_X , we have to extrapolate the inverse-Compton flux calculated for ν_{IC} by assuming the observed X-ray spectral index α_X . In the SSC case, we expect $\alpha_X \simeq \alpha_R$, if the synchrotron continuum can be well approximated by a single power-law with $\alpha \simeq \alpha_R$. The ratio of X-ray (SSC) luminosity to the radio (synchrotron) luminosity is therefore

$$\frac{\nu_{\text{IC}} f_{\text{IC}}}{\nu_R f_R} \simeq \frac{\nu_X f_X}{\nu_R f_R} \left(\frac{\nu_{\text{IC}}}{\nu_X} \right)^{1-\alpha_R} \simeq \frac{u'_{\text{sync}}}{u'_B}, \quad (8)$$

where u'_{sync} and u'_B are the synchrotron photon energy density and the magnetic field density, respectively, both evaluated in the emitting region rest frame denoted by primes. u'_{sync} is given by

$$\begin{aligned}u'_{\text{sync}} &= \frac{d_L^2 \nu_R f_R}{R^2 c \delta^4} = 7.9 \times 10^{-13} (1+z)^4 \left(\frac{\nu_R}{5\text{GHz}} \right) \\ &\quad \times \left(\frac{f_R}{100\text{mJy}} \right) \left(\frac{\theta}{0.3''} \right)^{-2} \delta^{-4} \quad [\text{erg/cm}^3],\end{aligned}\quad (9)$$

if we assume that the emission regions (jet-knots) are *moving* sources (see a discussion in Stawarz et al. 2004). From the equations (7)–(9), we predict the SSC flux density measured at ν_X to be roughly

$$\begin{aligned}
f_X &= 2.8 \times 10^{-3} \eta^{-1/2} (1+z) \left(\frac{d_L}{100 \text{Mpc}} \right)^{1/2} \\
&\times \left(\frac{\nu_R}{5 \text{GHz}} \right)^{5/4} \left(\frac{\nu_X}{\nu_{1 \text{keV}}} \right)^{-3/4} \left(\frac{f_R}{100 \text{mJy}} \right)^{3/2} \\
&\times \left(\frac{\theta}{0.3''} \right)^{-1/2} \delta^{-5/2} \quad [\text{nJy}].
\end{aligned} \tag{10}$$

Here we have assumed $\alpha_R = 0.75$ taking the result of Figure 1 into account. Note that f_X goes as $\propto \delta^{-5/2}$, meaning that the SSC flux significantly *decreases* as the beaming factor increases. Note also that $f_X \propto \theta^{-1/2}$, i.e. that for a given f_R and $B = B_{\text{eq}}$ clumping of the emission region leads to the *increase* of the SSC X-ray flux.

3.4. External Compton (EC) emission on CMB photon field

Similarly to the SSC case, we can estimate the expected EC flux at a certain X-ray frequency ν_X . In the EC model, electrons upscatter CMB photons to frequencies peaked at ν_{IC} , which, in a Thomson regime, is simply

$$\begin{aligned}
\nu_{\text{IC}} &\simeq \frac{4}{3} \gamma_R^2 \nu_{\text{CMB}} (1+z)^{-1} \delta^2 \kappa = 7.3 \times 10^{18} \eta^{-2/7} \\
&\times \kappa (1+z)^{-4/7} \left(\frac{d_L}{100 \text{Mpc}} \right)^{2/7} \left(\frac{\nu_R}{5 \text{GHz}} \right)^{6/7} \\
&\times \left(\frac{f_R}{100 \text{mJy}} \right)^{-2/7} \left(\frac{\theta}{0.3''} \right)^{6/7} \delta^{12/7} \quad [\text{Hz}],
\end{aligned} \tag{11}$$

where $\kappa = (1 + \mu)(1 + \beta)^{-1}$ and $\nu_{\text{CMB}} = 1.6 \times 10^{11} (1+z)$ [Hz]. Here we may set $\kappa \simeq 1$ for simplicity, since the value of κ is always an order of unity for any choice of Γ_{BLK} and δ . The ratio of X-ray (EC) luminosity to the radio (synchrotron) luminosity is approximately given by (Stawarz et al. 2003)

$$\frac{\nu_{\text{IC}} f_{\text{IC}}}{\nu_R f_R} \simeq \frac{\nu_X f_X}{\nu_R f_R} \left(\frac{\nu_{\text{IC}}}{\nu_X} \right)^{1-\alpha_R} \simeq \frac{u_{\text{CMB}}}{u'_B} \kappa^2 (1+z)^4 \delta^2, \tag{12}$$

where $u_{\text{CMB}} = 4.1 \times 10^{-13}$ erg/cm³. From the equations (11) and (12), the EC flux density measured at ν_X can be expressed as

$$\begin{aligned}
f_X &= 5.9 \times 10^{-4} \kappa^{7/4} \eta^{-1/2} (1+z) \left(\frac{d_L}{100 \text{Mpc}} \right)^{1/2} \\
&\times \left(\frac{\nu_R}{5 \text{GHz}} \right)^{1/2} \left(\frac{\nu_X}{\nu_{1 \text{keV}}} \right)^{-3/4} \left(\frac{f_R}{100 \text{mJy}} \right)^{1/2} \\
&\times \left(\frac{\theta}{0.3''} \right)^{3/2} \delta^3 \quad [\text{nJy}].
\end{aligned} \tag{13}$$

for $\alpha_R = 0.75$. It is interesting to note that f_X goes as $\propto \delta^3$, meaning that the EC flux significantly *increases* as the beaming factor increases, which is the exact opposite trend in the SSC case. Note also, that in the case of the EC emission $f_X \propto \theta^{3/2}$, i.e. for smaller emission region with given f_R and $B = B_{\text{eq}}$ the EC X-ray emission decreases, again opposite to what is expected in the case of the SSC process.

3.5. Source classification

First we group the sources by the X-ray spectral index α_X and the X-ray flux f_X observed at 1 keV. If the X-ray emission smoothly connects with the radio/optical spectra, we consider the X-rays to be produced via the synchrotron emission as for the radio to optical photons, and that only the highest energy tail of the electron population contributes to the X-ray emission. Good examples are the knots in M 87, where the X-ray spectral indices are $\alpha_X \simeq 1.3-1.6$ and the X-ray fluxes are consistent with radio-optical-X-ray synchrotron continua of a broken power-law form. As listed in Table 3, we find 25 ‘‘synchrotron’’ jet-knots and 7 hotspots, but none was found for the radio lobes. Figure 4 plots the distribution of $\gamma_X \delta^{1/7}$, calculated from the equation (5) derived in § 3.2. Note that for all the synchrotron sources, electrons must be accelerated very efficiently up to $\gamma_X \simeq 10^{7-8}$ for $B = B_{\text{eq}}$ (and to even higher energies if only $B < B_{\text{eq}}$), and that the highest population is occupied by the hotspots.

Meanwhile, remaining sources show flat X-ray spectra which cannot connect smoothly with the radio and optical spectra in terms of single (or broken) power-law continuum. Let us follow the ‘‘conservative’’ hypothesis that the X-rays in these sources are due to the inverse-Compton emission of either synchrotron itself (SSC), or the CMB

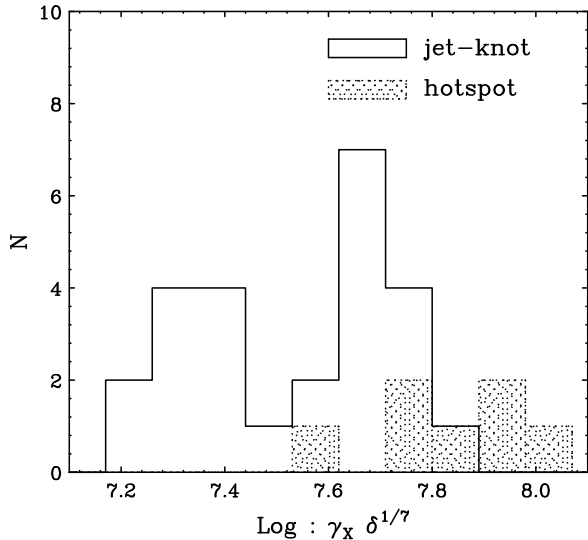


Fig. 4.— Distribution of the electron Lorentz factor, γ_x , for the SYN sources.

photons (EC). We therefore compare the ratio between the observed flux density to that expected one from SSC and EC models (c.f., § 3.3; 3.4), R_{SSC} and R_{EC} , to determine which process may dominate for the X-ray production. For example, the hotspot of 3C 123 is well explained by SSC, because $R_{\text{SSC}}(1) = 1.5$ and $R_{\text{EC}}(1) = 140$. This means that observed X-ray luminosity is 1.5 times larger than that expected from the SSC model under equipartition hypothesis, whereas 140 times of the expected EC flux if $\delta = 1$. In contrast, a good example of the EC source are the lobes in 3C 15, where $R_{\text{SSC}}(1) = 59$ and $R_{\text{EC}}(1) = 1.2$. The results of classification are given in the last column of Table 2.

Table 3. Source classification of Jets, hotspots, and lobes.

	Jet-knot	Hotspot	Lobe
QSO(CD)	19	2	0
QSO(LD)	7	9	6
RG(FR I)	22	0	3
RG(FR II)	1	13	9
BLZR	7	0	0
SYN	25	7	0
SSC	4	16	1
EC	27	1	17

Resultant group of jet-knots, hotspots and radio lobes are summarized in Table 3. Note that most of the jet-knots are either the synchrotron or the EC sources, whereas majority of the hotspots are the SSC sources. Moreover, almost all of the radio lobes emit X-rays via the EC (CMB) process. However, in a number of jet-knots classified as SSC and EC, the observed X-ray luminosities cannot be reproduced satisfactorily. For example, modelling of the jet-knot in PKS 0637 results in $R_{\text{SSC}}(1) = 600$ and $R_{\text{EC}}(1) = 1,600$, meaning that the observed X-ray flux is about 1,000 times brighter than those expected from both the EC and SSC models. As we have derived in § 3.3 and 3.4, and is well known from the literature, such discrepancy could be reduced by taking the relativistic beaming effect into account, $\delta \neq 1$, by giving up the equipartition hypothesis, $B < B_{\text{eq}}$, or by postulating a synchrotron origin of the X-ray photons due to an additional flat-spectrum electron population. None of these possibilities can be simply excluded. We will comment more about it in the next section.

Let us mention briefly, that due to differences in the model fitting procedure adopted in this paper as compared to the previous studies reported in the literature, some differences may occur in either specific values for the obtained model parameters (e.g., cf. Sambruna et al. 2004 for the case of NGC 6251), or even in classification of some particular sources (e.g., cf. Fabian et al. 2003 for 3C 9). Yet another case is the knot A1 in quasar 3C 273. Marshall et al. (2001) claimed that its X-ray emission is consistent with the extrapolation of the radio-to-optical single power-law synchrotron continuum. However, Jester et al. (2002) have shown that this is not the case, as the observed X-ray flux thereby *exceeds* the one expected from such an extrapolation. Here we classify the 3C 273 knot A1 as the SYN source, in accordance with Marshall et al. (2001), although it should be emphasized that – in face of the detailed optical studies by Jester et al. (2002, 2004) – this particular choice already involves non-standard energy distribution of the radiating electrons.

4. Discussion

In the previous sections, we have followed “conservative” classification of the discussed sources

based on their radio and X-ray emission properties. SYN sources are mainly found as jet-knots in nearby low-luminosity radio galaxies in agreement with previous studies (e.g., Hardcastle et al. 2001a, Pesce et al. 2001, Birkinshaw et al. 2002). If the magnetic field strength is not far from the equipartition value in these objects, the electrons must be accelerated very efficiently up to 10–100 TeV, in accordance with the general expectation that radio galaxies may be one of the most efficient particle accelerators in the Universe (see a discussion in Kataoka et al. 2003). If the electrons are actually accelerated to such high energies, the electrons emitting via synchrotron in the X-ray band have relatively short radiative life times. The synchrotron cooling time of the electrons can be expressed as

$$t_{\text{sync}} = 250 \left(\frac{B_{\text{eq}}}{100 \mu\text{G}} \right)^{-2} \left(\frac{\gamma}{10^7} \right)^{-1} \text{ [yr]}. \quad (14)$$

Since Comptonization of the synchrotron photons, CMB photons and of the galactic photon fields also cool electrons (what can be especially significant if the considered jets are relativistic on kpc scales), the above estimate would be an upper limit for the electron cooling time scale. Indeed, Stawarz et al. (2003) estimated the energy density of the starlight emission at 1 kpc from the center of average elliptical galaxy – where typically the X-ray bright knots of the low-powerful jets are located – to be $u_{\text{star}} \sim 10^{-9} \text{ erg cm}^{-3}$. Now, for the 25 FR I jet-knots classified as SYN sources in this paper the median equipartition magnetic field computed for non-relativistic bulk velocities is $B_{\text{eq}, \delta=1} = 130 \mu\text{G}$ (see Table 2), what gives the comoving energy density of the magnetic field $u'_B = 6.7 \times 10^{-10} \delta^{-10/7} \text{ erg cm}^{-3}$. Thus, the relative importance of the inverse-Compton to synchrotron radiative losses for the electrons within the FR I jets is roughly

$$\frac{u'_{\text{star}}}{u'_B} \sim \Gamma_{\text{BLK}}^2 \delta^{10/7}. \quad (15)$$

That is, radiating electrons within nearby FR I jets possessing X-ray (and optical) counterparts (which are believed to be at least moderately beamed toward the observer, $\delta > 1$), cool mainly due to inverse-Compton losses on the starlight photon fields of the host galaxies unless $B \gg B_{\text{eq}}$.

Hence, for the highest energy electrons in the FR I jets one can safely put the radiative cooling spatial scale $ct_{\text{cool}} < 100 \text{ pc}$. In general, this is consistent with the visual sizes of the jet-knots, but significantly smaller than the typical knots' distances from the nucleus ($\gtrsim \text{kpc}$ in the case of FR I sources), and also than the typical inter-knot separation distances. Therefore, the jet electrons have to be accelerated *in situ*, most probably due to stochastic processes connected with strong turbulence occurring within those jets as a result of the mass entrainment from the surrounding medium (De Young 1986).

One can ask if in the case of the SYN jet-knots in the nearby FR I galaxies magnetic field can be much smaller than the equipartition value. This possibility could be verified by means of detecting the inverse-Compton radiation of the synchrotron-emitting electrons, which is expected to peak at high-energy γ -ray band. Interestingly, we can already put some meaningful limits on such high-energy component in the case of the M 87 jet. Nearby radio galaxy M 87 was detected at TeV photon energies by *HEGRA* Cherenkov Telescope (Aharonian et al. 2003), and it was shown that the kpc-scale jet in this object can produce very high energy γ -ray photons at the required level via comptonization of the starlight photon field (Stawarz et al. 2003). However, the latest non-detection of M 87 by *Whipple* Telescope (Le Bohec et al. 2004) suggests variability of the discussed TeV radiation, indicating that the kpc-scale jet in M 87 cannot account for the *HEGRA* signal. The implied upper limits indicate in turn that the magnetic field within the kpc-scale jet of M 87 radio galaxy cannot be smaller than the equipartition value (Stawarz et al. 2004, in preparation). Thus, one can expect that also in the case of the other FR I jets $B \gtrsim B_{\text{eq}}$.

For the SSC and EC sources, a number of jet-knots seem extremely bright in the X-rays, as we have seen in Figure 2 and 3. This inevitably causes a large discrepancy between the “expected” and “observed” X-ray fluxes as we see in Table 2 and § 3.5, and what is again well known from the previous studies. One formal possibility is that equipartition hypothesis may not be valid in the considered jet-knots. For a given synchrotron luminosity $L_{\text{sync}} \propto u_e u_B$ and for a given emitting region volume V , an expected SSC luminosity is $L_{\text{SSC}} \propto$

u_e . We therefore expect ratio $R_{\text{SSC}}(1) \propto L_{\text{SSC}}^{-1} \propto u_B$. Similarly, for the EC case, $R_{\text{EC}}(1) \propto L_{\text{EC}}^{-1} \propto u_B$. Hence, in both models, the expected X-ray luminosity will be increased by decreasing the magnetic field strength.

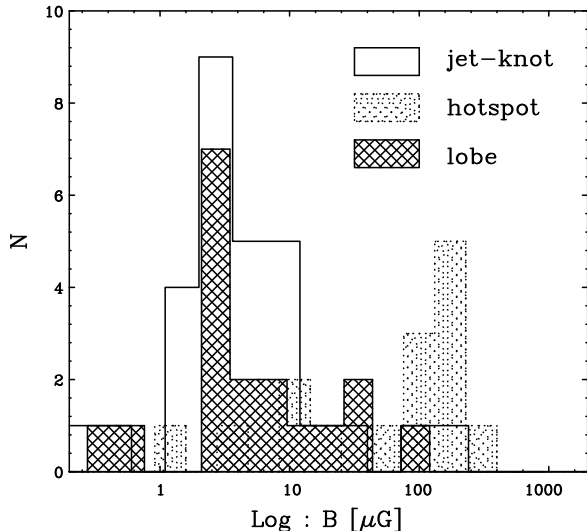


Fig. 5.— Distribution of the evaluated magnetic field, B , for the case of *no* relativistic beaming ($\delta=1$).

Figure 5 shows the distribution of the “best-fit” magnetic field B if we allow for the deviation from the equipartition condition and assume nonrelativistic velocities for the emitting regions (what, in the case of the jet-knots, is rather only a formal hypothesis). One finds that both the non-SYN jet-knots and radio lobes are distributed around $B \simeq 1\text{--}10\mu\text{G}$, whereas hotspots have a relatively narrow peak at higher field strength, $B \simeq 50\text{--}300\mu\text{G}$, plus a “tail” extending down to $\sim\mu\text{G}$. Figure 6 shows the ratio of B to the equipartition value. Interestingly, B in the lobe and most of the hotspots are almost consistent with the equipartition ($B/B_{\text{eq},\delta=1} \sim 1$), whereas that of the non-SYN jet-knots and of some of the hotspots is much weaker from what is expected ($B/B_{\text{eq},\delta=1} \sim 0.01\text{--}0.1$).

As an alternative idea, we also consider a case when the difference between the “expected” and “observed” X-ray fluxes is due to the relativistic beaming effect, and the minimum-power condition is fulfilled, as suggested by Tavecchio et al. (2000) and Celotti et al. (2001). Relativistic beaming

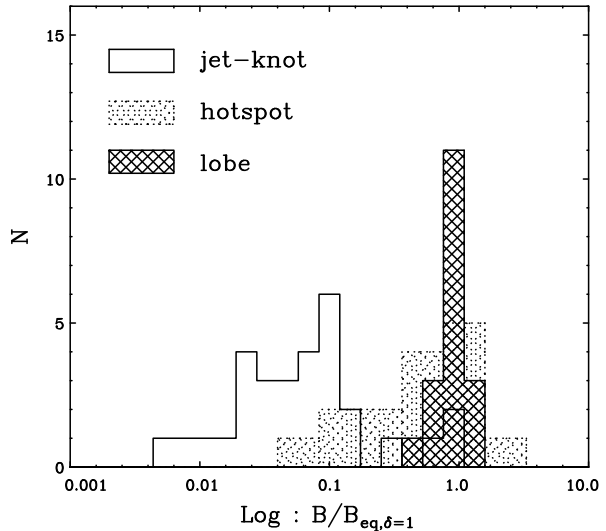


Fig. 6.— Distribution of the ratio between the evaluated magnetic field B (for $\delta = 1$) and the equipartition value $B_{\text{eq},\delta=1}$.

changes the observed X-ray luminosities significantly as $f_X \propto \delta^{-5/2}$ for the SSC and $\propto \delta^3$ for the EC (equation (10) and (13)). Deviation from equipartition may not be formally required so long as an appropriate beaming factor is assumed. The Doppler factors thus calculated are shown in Table 2 and Figure 7. One can see that the lobes and the hotspots exhibit relatively narrow distribution at $\delta \sim 1$, whereas for most of the jet-knots large beaming factors of ~ 10 are required, as noted before by many authors. We note, that the obtained $\delta \sim 0.1$ for some of the hotspots is rather a formal possibility. Figure 8 shows the distribution of equipartition magnetic field in the framework of relativistically moving jet model. Similarly to Figure 5, we find again that the narrowly distributed strength of the magnetic field in the hotspots, $B \sim 100\text{--}500\mu\text{G}$, is an order of magnitude larger than that of the jet-knots and radio lobes.

Apparently, the above considerations imply that the inverse-Compton X-ray emissions from the lobes and hotspots are relatively close to that expected from the magnetic field–radiating electrons energy equipartition, with at most mildly-relativistic bulk velocities of the radiating plasma. A number of jet-knots in powerful sources requires however significant bulk Lorentz factor of $\Gamma_{\text{BLK}} \geq \delta/2 \sim 5$ to agree the inverse-Compton origin

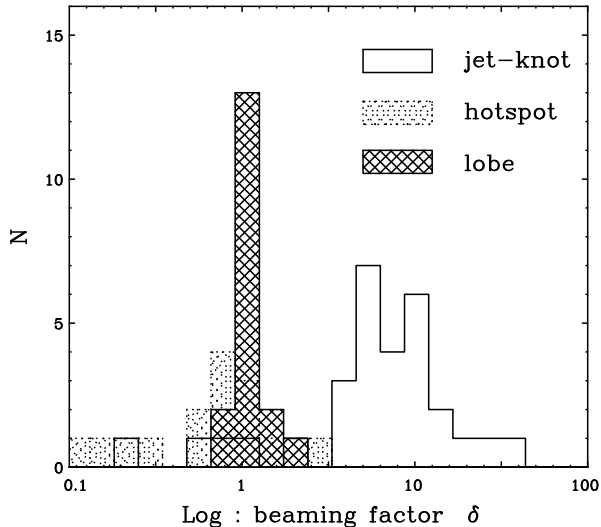


Fig. 7.— Distribution of the required beaming factor δ for $B = B_{\text{eq}}$.

of the X-ray photons with the minimum-power condition $B = B_{\text{eq}}$. We note, that our evaluation gives the *minimum* value of B_{eq} , as we set $\nu_{\text{min}} = \nu$ in the equation (1) and $\eta = 1$ in the subsequent analysis. Therefore, any more realistic derivation would result in an even larger deviation from the energy equipartition, and thus in an even larger value for the jet Doppler factor δ required to satisfy the minimum power condition. Let us mention, that the alternative two-population synchrotron models do not require violation of the energy equipartition (Stawarz & Ostrowski 2002, Dermer & Atoyan 2004).

Usually, in applying the EC model to the quasar jet-knots' X-ray emission, the idea of sub-equipartition magnetic field is rejected since it implies a very high kinetic power of the jets. For this reason, large values for the jet Doppler factors are invoked. However, as discussed by, e.g., Atoyan & Dermer (2004), such an approach does not solve all the problems with the total energy requirements (see also a discussion in Stawarz 2004). Let us mention in this context another important issue. It is well known, that the *VLA* studies of the large-scale jets in quasars and FR IIs indicate that bulk Lorentz factors of the radio-emitting plasma in these sources cannot be much greater than $\Gamma_{\text{BLK}} \sim 3$ (Wardle & Aaron 1997). The discrepancy between this result and the re-

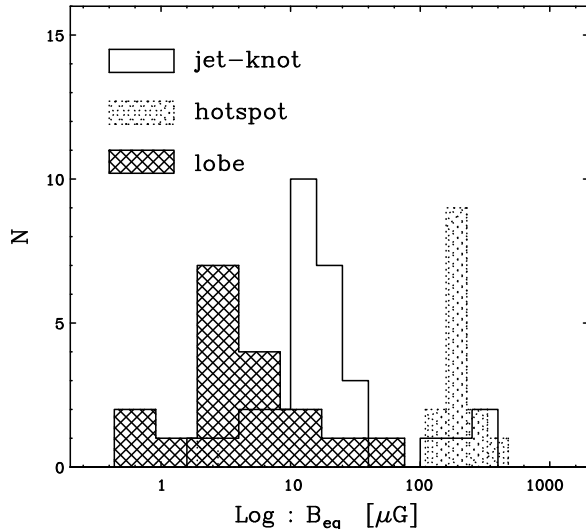


Fig. 8.— Equipartition magnetic field for relativistically moving jet model.

quirement of the minimum-power EC model for $\Gamma_{\text{BLK}} > 10$ is typically ascribed to the jet radial velocity structure, namely that the radio emission originates within slower-moving jet boundary layer and the inverse-Compton X-ray radiation is produced within the fast jet spine (e.g., Ghisellini & Celotti 2001). While it is true that jet radial stratification can indeed significantly influence jet-counterjet brightness asymmetry ratio, one should be aware that by postulating different sites for the origin of radio and X-ray photons, homogeneous one-zone models for the broad-band knots' emission can no longer be preserved. In particular, in such a case one has to specify exactly what fraction of the jet radio emission is produced within the spine and what fraction within the boundary layer, what is exactly the jet velocity radial profile, and what is the magnetic field strength in each jet components, etc. Without such a discussion one cannot simply use the observed radio flux of the jet to construct the broad-band spectral energy distribution of the knot region, i.e. simply estimate the expected inverse-Compton flux by means of equipartition magnetic field derived from the radio observations. If one insists on applying the homogeneous one-zone model (as a zero-order approximation), as presented in this paper, self-consistency requires a consideration of $\Gamma_{\text{BLK}} \leq 5$. In such a case, a departure from the

minimum power conditions within the non-SYN X-ray jets is *inevitable*.

Accordingly to the discussion above, if the X-ray emission of the powerful jets is due to the EC process, these jets are most likely *particle dominated* ($u_e \gg u_B$). The jet magnetic field must be then significantly amplified in the hotspot, where an approximate equipartition is expected to be reached. Then the shocked plasma moves slowly to the radio lobe, where the equipartition field becomes close to the intergalactic value ($B \sim$ a few μG). Let us comment in this context on the following issue. Pressure of radio-emitting electrons within the lobes of quasars and FR IIs computed from the equipartition condition is often found to be below the thermal pressure of the ambient medium (Hardcastle & Worrall 2000), what challenges the standard model for the evolution of powerful radio sources. Such a discrepancy can be removed only by postulating deviations from the equipartition condition, or presence of non-radiating relativistic protons within the lobes. The presented analysis of the X-ray data confirms for a large number of sources the anticipated result that the magnetic field–radiating electrons energy equipartition within the lobes is generally fulfilled, and thus that the relativistic protons are very likely to constitute a significant fraction of the lobes’ non-thermal pressure. Interestingly, this would mean that the total energy outputs of powerful jets are systematically *larger* from what is implied by the analysis of the lobes’ radio emission solely (Rawlings & Saunders 1991). This, in turn, would be consistent with deviation from the minimum-power condition within the considered jets themselves. We note that viscous acceleration of cosmic rays taking place at the turbulent boundary layers of relativistic jets, discussed by, e.g., Ostrowski (2000) and Rieger & Mannheim (2002), could provide energetically important flat-spectrum population of ultrarelativistic protons within the lobes of powerful radio sources.

We have discussed two different versions of the EC model to account for extremely bright X-ray jet-knots: (1) non-equipartition case and (2) significant relativistic beaming case. Both of these options are in many ways problematic. Our next concern is to attempt to prove in general the postulated inverse-Compton origin of the X-ray pho-

tons. Note in this context, that for the EC sources the radio-to-X-ray flux ratio is proportional to $u'_B{}^{-1}(1+z)^4\delta^2$ (equation 12). Therefore, for a large sample of EC sources one should expect to observe $L_R/L_X \propto (1+z)^4$ behavior, if only B and Γ_{BLK} do not have large scatter from source-to-source (cf. Figures 5 and 7). We therefore expect the high-redshift EC sources to be brighter in X-rays than nearby EC sources (see Schwartz 2002, Cheung 2004).

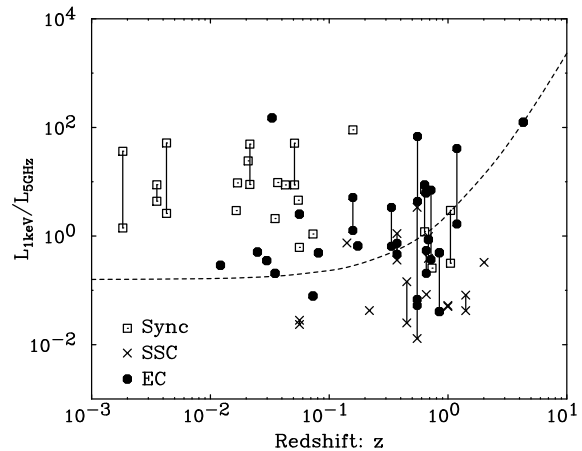


Fig. 9.— Luminosity ratio, $L_{1\text{keV}}/L_{5\text{GHz}}$, as a function of redshift for SYN, SSC and EC sources.

Figure 9 shows the distribution of the flux ratio ($L_{1\text{keV}}/L_{5\text{GHz}}$) as a function of z . The dotted line shows $\propto (1+z)^4$ relation which fits the highest z data point (GB 1508+5714; $z = 4.3$) just to help guide the eyes. Although data sample is still poor, we may say that no clear trend can be seen in this plot. Furthermore, we notice that the discussed ratio is widely distributed even in the same objects. For example, in cases of knots in 4C 19.33 ($z = 0.72$), “conservatively” classified as the EC sources, the X-ray-to-radio luminosity ratio changes of about an order of magnitude (Table 2). Such a difference is not easy to explain in the framework of model (1), since we have to assume an order of magnitude increase in the magnetic fields along the jet. In a framework of relativistic beaming hypothesis (2) one may possibly explain such variation by postulating the decrease of the bulk Lorentz factor along the flow and only moderate changes in magnetic field (Georganopoulos & Kazanas 2004). In this case, however, one has to explain what causes significant deceleration of the

jet, which preserves its excellent collimation, with no significant radiative energy losses. We need more data obtained in various energy bands, and a more sophisticated analysis to conclude this further. However, we note that recent observations of high-redshift quasars by Bassett et al. (2004) did not reveal any evidence for the enhanced X-ray emission of the distant large-scale jets due to the increased energy density of the cosmic microwave background. Since such an effect is expected in a framework of the EC model, one may conclude that the X-ray photons from the powerful quasar jets are not inverse-Compton in origin. Recent detailed re-analysis of the *Chandra* data for 3C 120, again “conservatively” classified as an EC source, strongly support this idea (Harris et al. 2004).

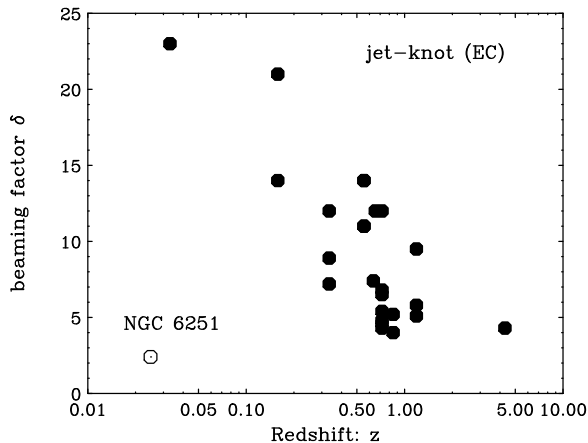


Fig. 10.— Expected beaming factor δ_{EC} for $B = B_{\text{eq}}$, as a function of redshift for EC jet-knot sources. *Open circle* shows FR I radio galaxy NGC 6251, but its X-ray emission seems to be problematic in a framework of the EC model. Full details are given in the text.

Let us finally discuss yet another issue regarding the EC scenario for the quasar jets’ X-ray emission. Figure 10 shows the Doppler beaming factor δ required in this model to obtain $B = B_{\text{eq}}$, versus the redshifts z of the jet-knots classified here as the EC ones. One can clearly see a significant anticorrelation between δ and z , meaning that the high- z sources require much smaller δ for the magnetic field-radiating electrons energy equipartition than the sources located closer to the observer.¹

¹Nearby FR I radio galaxy NGC 6251 (*open circle*) consti-

There are two possible explanations for the noted δ - z anticorrelation. If reflecting physical property, it would mean that the distant large-scale quasar jets are less relativistic than their nearby analogues but similarly close to the equipartition, or that both low- and high- z quasar jets are only mildly relativistic on large scales but closer to the minimum-power condition when located at large redshifts. None of this options appear to be particularly inartificial, especially as the high- z quasar cores seem to be comparable to their low- z counterparts (e.g., Bassett et al. 2004). On the other hand, differences in velocity and energy content of the large-scale jets may not reflect differences in the central engines, but more likely differences in the surrounding galactic or intergalactic medium. The second possibility for understanding δ - z anticorrelation is however that it is simply an artifact of the applied but inappropriate EC model. This issue has to be discussed carefully for a larger number of sources.

5. Conclusion

We have studied the statistical properties of the large-scale jet-knots, hotspots and lobes in more than 40 radio galaxies recently observed with *Chandra* and *ASCA*. For the jet-knots in nearby low-luminosity radio galaxies and for some of the hotspots, X-ray photons are most likely synchrotron in origin, being then produced by ultrarelativistic electrons with energies 10–100 TeV that must be accelerated in situ. For the other objects X-ray photons are inverse-Compton in origin, or, alternatively, are due to synchrotron emission of very high energy electrons with a non-standard energy distribution. In this paper we examine in more detail the former possibility. We first calculated the “expected” SSC or EC fluxes by assuming equipartition magnetic field and nonrelativistic velocity of the emitting plasma, and then compared them to the observed fluxes. We confirmed that the observed X-ray fluxes from the hotspots and radio lobes are approximately consistent with the expected ones, whereas a number of the jet-knots in powerful sources is too

tutes the only exception from this trend. However, this peculiar source does not belong to the quasar class, and, in general, its X-ray emission is particularly problematic (especially in a framework of the EC model).

bright at X-rays. We examined two possibilities to account for this discrepancy in a framework of the inverse-Compton model. The first idea is that equipartition hypothesis may not be valid for the considered sources. In this case, the X-ray bright jets are particle dominated and therefore far from the minimum-power condition. The jet magnetic field must be then significantly amplified in the hotspots where an approximate energy equipartition with the radiating particles is expected to be reached. An alternative idea is that the jets are highly relativistic ($\Gamma_{\text{BLK}} \geq 5$) even on kpc/Mpc scales, but significantly decelerate in the hotspots. This however, in addition to other problems, challenges the homogeneous one-zone emission region model adopted in this paper, as discussed in the text. Unfortunately, the comparison of the observed radio-to-X-ray flux ratios for various z sources *from the compiled dataset* does not provide definite constraints on the X-ray emission process dominating within the quasar and FR II jets.

We would like to thank F. Takahara and M. Ostrowski for fruitful discussion and constructive comments. J.K. acknowledges a support by JSPS.KAKENHI (14340061). L.S. was supported by the grant PBZ-KBN-054/P03/2001 and partly by the Chandra grants G02-3148A and G0-09280.01-A.

REFERENCES

- Aharonian, F. A., 2002, MNRAS, 332, 215
- Aharonian, F. A., et al., 2003, A&A, 403, L1
- Akujor, C. E., Spencer, R. E., Zhang, F. J., Davis, R. J., Browne, I. W. A., & Fanti, C., 1991, MNRAS, 250, 215
- Aldcroft, T. L., Siemiginowska, A., Elvis, M., Mathur, S., Nicastro, F., & Murray, S. S., 2003, ApJ, 597, 751
- Aloy, M. A., Ibanez, J. M., Marti, J. M., Gomez, J.-L., & Müller, E., 1999, ApJ, 523, L125
- Atoyan, A. M., & Dermer, C. D., 2004, ApJ, accepted (astro-ph/0402647)
- Bałucińska-Church, M., Ostrowski, M., Stawarz, L., & Church, M. J., 2004, MNRAS, submitted
- Bassett, L. C., Brandt, W. N., Schneider, D. P., Vignali, C., Chartas, G., & Garmire, G. P., 2004, AJ, 128, 523
- Birkinshaw, M., Worrall, D. M., & Hardcastle, M. J., 2002, MNRAS, 334, 182
- Blundell, K. M., & Rawlings, S., 2000, AJ, 119, 1111
- Bridle, A. H., Hough, D. H., Lonsdale, C. J., Burns, J. O., Laing, R. A., 1994, ApJ, 108, 766
- Brunetti, G., Setti, G., & Comastri, A., 1997, A&A, 325, 898
- Brunetti, G., Cappi, M., Setti, G., Feretti, L., & Harris, D. E., 2001a, A&A, 372, 755
- Brunetti, G., Bondi, M., Comastri, M., Pedani, M., Varano, S., Setti, G., & Hardcastle, M. J., 2001b, ApJ, 561, L157
- Brunetti, G., Bondi, M., Comastri, A., & Setti, G., 2002, A&A, 381, 795
- Celotti, A., Ghisellini, G., & Chiaberge, M., 2001, MNRAS, 321, L1
- Chartas, G., et al., 2000, ApJ, 542, 655
- Chartas, Gupta, V., Garmire, G., Jones, C., Falco, E. E., Shapiro, I. I., & Tavecchio, F., 2002, ApJ, 565, 96
- Cheung, C. C., 2004, ApJ, 600, L23
- Comastri, A., Brunetti, G., Dallacasa, D., Bondi, M., Pedani, M., & Setti, G., 2003, MNRAS, 340, 52
- De Young, D. S., 1986, ApJ, 307, 62
- De Young, D. S., 2002a, *'The Physics of Extragalactic Radio Sources'*, University of Chicago Press
- De Young, D. S., 2002b, NewAR, 2002b, 46, 393
- Dermer, C. D., & Atoyan, A. M., 2002, ApJ, 568, 81
- Dermer, C. D., & Atoyan, A. M., 2004, ApJ, 611, 9
- Donahue, M., Daly, R. A., & Horner, D. J., 2003, ApJ, 584, 643

- Fabian, A. C., Celotti, A., & Johnstone, R. M., 2003, MNRAS, 338, L7
- Georganopoulos, M., & Kazanas, D., 2004, ApJ, 604, 81
- Ghisellini, G., & Celotti, A., 2001, MNRAS, 327, 739
- Hardcastle, M. J., & Worrall, D. M., 2000, MNRAS, 319, 562
- Hardcastle, M. J., Alexander, P., Pooley, G. G., & Riley, J. M., 1997, MNRAS, 288, 859
- Hardcastle, M. J., Birkinshaw, M., & Worrall, D. M., 2001a, MNRAS, 326, 1499
- Hardcastle, M. J., Birkinshaw, M., & Worrall, D. M., 2001b, MNRAS, 323, L17
- Hardcastle, M. J., Worrall, D. M., Birkinshaw, M., Laing, R. A., & Bridle, A. H., 2002a, MNRAS, 334, 182
- Hardcastle, M. J., Birkinshaw, M., Cameron, R. A., Harris, D. E., Looney, L. W., & Worrall, D. M., 2002b, ApJ, 581, 948
- Hardcastle, M. J., Harris, D. E., Worrall, D. M., & Birkinshaw, M., 2004, ApJ, in press (astro-ph/0405516)
- Harris, D. E., & Krawczynski, H., 2002, ApJ, 565, 244
- Harris, D. E., Krawczynski, H., & Taylor, G. B., 2002, ApJ, 578, 60
- Harris, D. E., Leighly, K., & Leahy, J. P., 1998, ApJ, 499, L149
- Harris, D. E., Mossman, A. E., & Walker, R. C., 2004, ApJ, accepted (astro-ph/0407354)
- Harris, D. E., Hjorth, J., Sadun, A. C., Silverman, J. D., & Vestergaard, M., 1999, ApJ, 518, 213
- Harris, D. E., et al., 2000, ApJ, 530, L81
- Harris, D. E., Finoguenov, A., Bridle, A. H., Hardcastle, M. J., & Laing, R. A., 2002, ApJ, 580, 110
- Harvanek, M., Stocke, J. T., Morse, J. A., & Rhee, G., 1997, AJ, 114, 2240
- Isobe, N., Ph. D. Thesis, 2002, University of Tokyo
- Isobe, N., Tashiro, M., Makishima, K., Iyomoto, N., Suzuki, M., Murakami, M., Mori, M., & Abe, K., 2002, ApJ, 580, L111
- Jester, S. 2003, NewAR, 47, 427
- Jester, S., Röser, H.-J., Meisenheimer, K., & Perley, R. 2002, A&A, 385, L27
- Jester, S., Röser, H.-J., Meisenheimer, K., & Perley, R. 2004, A&A, accepted (astro-ph/0410520)
- Kaiser, C. R. 2000, A&A, 362, 447
- Kataoka, J., Edwards, P., Georganopoulos, M., Takahara, F., & Wagner, S., 2003a, A&A, 399, 91
- Kataoka, J., Leahy, J. P., Edwards, P. G., Kino, M., Takahara, F., Serino, Y., Kawai, N., & Martel, A. R., 2003b, A&A, 410, 833
- Kirk, J. G., & Duffy, P., 1999, J. Phys. G, 25, 163
- Komissarov, S. S. 1999, MNRAS, 308, 1069
- Kraft, R. P., Forman, W. R., Jones, C., Murray, S. S., Hardcastle, M. J., & Worrall, D. M., 2002, ApJ, 569, 54
- Laing, R. A & Bridle, A. H., 2002, MNRAS, 336, 328
- Le Bohec, S., et al., 2004, ApJ, 610, 156
- Leahy, J. P., Black, A. R. S., Dennett-Thorpe, J., Hardcastle, M. J., Komissarov, S., Perley, R. A., Riley, J. M., & Scheuer, P. A. G., 1997, MNRAS, 291, 20
- Longair, M. S. 1994, *High Energy Astrophysics*, Cambridge Univ. Press, Cambridge
- Manolakou, K., & Kirk, J. G., 391, 127
- Marshall, H. L., et al., 2001, ApJ, 549, L167
- Marshall, H. L., Miller, B. P., Davis, D. S., Perleman, E. S., Wise, M., Canizares, C. R., & Harris, D. E., 2002, ApJ, 564, 683
- Marti, J. M. A., Müller, E., Font, J. A., Ibanez, J. M. A., & Marquina, A., 1007, ApJ, 479, 151

- Meisenheimer, K., Yates, M. G., & Roeser, H. -J. 1997, *A&A*, 325, 57
- Mizuta, A., Yamada, S., & Takabe, H., 2004, *ApJ*, 606, 804
- Ostrowski, M., 2000, *MNRAS*, 312, 579
- Ostrowski, M., 2002, *J. Phys. Stud.*, 6, 393
- Perlman, E. S., Biretta, J. A., Sparks, W. B., Macchetto, F. D., & Leahy, J. P., 2001, *ApJ*, 551, 206
- Pesce, J. E., Sambruna, R. M., Tavecchio, F., Maraschi, L., Cheung, C. C., Urry, C. M., & Scarpa, R., 2001, *ApJ*, 556, L79
- Rawlings, S., & Saunders, R., 1991, *Nature*, 349, 138
- Rieger, F. M., & Mannheim, K., 2002, *A&A*, 396, 833
- Sambruna, R. M., Urry, C. M., Tavecchio, F., Maraschi, L., Scarpa, R., Chartas, G., & Muxlow, T., 2001, *ApJ*, 549, L161
- Sambruna, R. M., Maraschi, L., Tavecchio, F., Urry, C. M., Cheung, C. C., Chartas, G., Scarpa, R., Gambill, J. K., 2002, *ApJ*, 571, 206
- Sambruna, R. M., Gliozzi, M., Donato, D., Tavecchio, F., Cheung, C. C., & Mushotzky, R. F., 2004, 414, 885
- Scarpa, R., & Urry, C. M., 2002, *NewAR*, 46, 405
- Schwartz, D. A., 2002, *ApJ*, 569, L23
- Schwartz, D. A., et al., 2000, *ApJ*, 540, L69
- Siemiginowska, A., Bechtold, J., Aldcroft, T. L., Elvis, M., Harris, D. E., & Dobrzycki, A., 2002, *ApJ*, 570, 543
- Siemiginowska, A., et al., 2003a, *ApJ*, 595, 643
- Siemiginowska, A., Smith, R. K., Aldcroft, T. L., Schwartz, D. A., Paerels, F., Petric, A., O., 2003b, *ApJ*, 598, L15
- Sikora, M., & Madejski, G., 2000, *ApJ*, 534, 109
- Sparks, W. B., Golombek, D., Baum, S. A., Biretta, J., de Koff, S., Macchetto, F., McCarthy, P., & Miley, G. K., 1995, *ApJ*, 450, L55
- Stawarz, L., 2004, *ChJAA*, in press (*astro-ph/0310795*)
- Stawarz, L., & Ostrowski, M., 2002, *ApJ*, 578, 763
- Stawarz, L., Sikora, M., Ostrowski, M., 2003, *ApJ*, 597, 186
- Stawarz, L., Sikora, M., Ostrowski, M., & Begelman, M. C., 2004, *ApJ*, 608, 95
- Tashiro, M., et al., 1998, *ApJ*, 499, 713
- Tashiro, M., Makishima, K., Iyomoto, N., Isobe, N., & Kaneda, H., 2001, *ApJ*, 546, L19
- Tavecchio, F., Maraschi, L., Sambruna, R. M., and Urry, C. M., 2000, *ApJ*, 544, L23
- Wardle, J. F. C., & Aaron, S. E., 1997, *MNRAS*, 286, 425
- Wilson, A. S., Young, A. J., & Shopbell, P. L., 2001, *ApJ*, 547, 740
- Wilson, A. S., Young, A. J., & Shopbell, P. L., 2000, *ApJ*, 544, L27
- Wilson, A. S., & Yang, Y., 2002, *ApJ*, 568, 133
- Worrall, D. M., Birkinshaw, M., & Hardcastle, M. J., 2001, *MNRAS*, 326, L7
- Worrall, D. M., Birkinshaw, M., & Hardcastle, M. J., 2003, *MNRAS*, 343, L73
- Yuan, W., Fabian, A. C., Celotti, A., & Jonker, P. G., 2003, *MNRAS*, 346, L7

TABLE 1
LIST OF RADIO SOURCES WITH EXTENDED X-RAY JET, HOTSPOT, AND LOBE STRUCTURES

name	z	d_L [Mpc] ^a	class ^b	reference
3C 9	2.012	16133	QSO(LD)	Bridle et al. 1994, Fabian, Celotti & Johnstone 2003
3C 15	0.073	302	RG(FR I)	Leahy et al. 1997; Kataoka et al. 2003b
NGC315	0.0165	67	RG(FR I)	Worrall, Birkinshaw & Hardcastle 2003
3C 31	0.0169	67	RG(FR I)	Laing & Bridle 2002; Hardcastle et al. 2002a
NGC 612	0.0298	120	RG(FR II)	Isobe 2002
B0206+35	0.0369	150	RG(FR I)	Worrall, Birkinshaw & Hardcastle 2001
3C66B	0.0215	87	RG(FR I)	Hardcastle, Birkinshaw & Worrall 2001a
Fornax A	0.00587	23.5	RG(FR I)	Tashiro et al. 2001
3C 120	0.033	134	RG(FR II)	Harris et al. 1999; 2004
3C 123	0.218	965	RG(FR II)	Hardcastle et al. 1997; Hardcastle, Birkinshaw, & Worrall, 2001b
3C 129	0.0208	84	RG(FR I)	Harris, Krawczynski & Taylor 2002
Pictor A	0.035	143	RG(FR II)	Wilson, Young & Shoppbell 2001; Isobe 2002
PKS0521-365	0.055	225	BLZR	Birkinshaw, Warrall & Hardcastle 2002
PKS0637-752	0.653	3465	BLZR	Chartas et al. 2000; Schwartz et al. 2000
3C 179	0.846	4815	QSO(LD)	Sambruna et al. 2002
B2 0738+313	0.635	3344	QSO(CD)	Siemiginowska et al. 2003a
B2 0755+37	0.0428	175	RG(FR I)	Worrall Birkinshaw & Hardcastle 2001
3C 207	0.684	3642	QSO(LD)	Brunetti et al. 2002
3C 212	1.049	6393	QSO(LD)	Akujor et al. 1991, Aldcroft et al. 2003
3C 219	0.174	756	RG(FR II)	Comastri et al. 2003
4C73.08	0.0581	236	RG(FR II)	Isobe 2002
Q0957+561	1.41	9613	QSO(CD)	Harvanek et al.1997; Chartas et al.2002
3C 254	0.734	4011	QSO(LD)	Donahue, Daly & Horner 2003
PKS1127-145	1.187	7505	QSO(CD)	Siemiginowska et al. 2002
PKS1136-135	0.554	2830	QSO(LD)	Sambruna et al. 2002
3C 263	0.656	3487	QSO(LD)	Hardcastle et al. 2002b
4C 49.22	0.334	1559	QSO(CD)	Sambruna et al. 2002
M 84	0.00354	11.3	RG(FR I)	Harris et al. 2002
3C 273	0.1583	683	BLZR	Marshall et al. 2001; Sambruna et al. 2001
M87	0.00427	10.7	RG(FR I)	Marshall et al. 2002; Wilson & Yang 2002; Perlman et al. 2001
3C 280	0.996	5964	RG(FR II)	Donahue, Daly & Horner 2003
Cen A	0.00183	2.3	RG(FR I)	Kraft et al. 2002
Cen B	0.01215	48.7	RG(FR I)	Tashiro et al. 1998
4C19.44	0.720	3917	QSO(CD)	Sambruna et al. 2002
3C 295	0.45	2205	RG(FR II)	Harris et al. 2000; Brunetti et al. 2001a
3C 303	0.141	603	RG(FR II)	Meisenheimer, Yates & Roeser 1997; Kataoka et al. 2003a
GB1508+5714	4.3	54142	QSO(CD)	Siemiginowska et al.2003b; Yuan et al. 2003; Cheung 2004
3C 330	0.55	2803	RG(FR II)	Hardcastle et al. 2002b
NGC6251	0.0249	101	RG(FR I)	Sambruna et al.2004
3C 351	0.372	1763	QSO(LD)	Brunetti et al.2001b; Hardcastle et al. 2002b
3C 371	0.051	209	BLZR	Pesce et al. 2001
3C 390.3	0.0561	230	RG(FR II)	Harris, Leighly & Leahy 1998; this work
Cyg A	0.0562	231	RG(FR II)	Wilson, Young & Shoppbell 2000
3C 452	0.0811	331	RG(FR II)	Isobe et al. 2002

^a d_L : Luminosity distance to the source adopting $H_0 = 75 \text{ km s}^{-1} \text{ Mpc}^{-1}$ and $q_0 = 0.5$.

^bRG; radio galaxy of either Fanaroff & Riley type I (FR I) or type II (FR II), QSO: quasar of either core dominated (CD) or lobe dominated (LD), and BLZR: blazars.

TABLE 2
PARAMETERS FOR X-RAY JET, HOTSPOT, AND LOBE FEATURES

name	comp	α_R	f_R [mJy]	α_X	f_X [nJy]	f_O [μ Jy]	θ [$^\circ$]	$B_{eq}(1)$ [μ G]	$R_{SSC}(1)$	$R_{EC}(1)$	δ_{SSC}	δ_{EC}	class
3C9	K	1.0f	3.2e2	0.6 \pm 0.6	2.2	–	0.3f	230	3.6	54	0.60	3.8	SSC
3C15	K-C	0.9	55	0.7 \pm 0.4	1.2	6.0	0.3f	84	5.5e2	1.5e3	0.080	11	SYN
	L	0.8	1.8e3	0.3 \pm 0.4	2.9	–	20	6.2	58	1.1	0.20	1.0	EC
NGC315	K	0.9f	68	1.5 \pm 0.7	4.1	–	0.3f	130	3.1e3	1.0e4	0.040	22	SYN
3C31	K	0.55	37	1.1 \pm 0.2	7.3	2.0	0.3f	110	1.4e4	2.4e4	0.022	29	SYN
NGC612	L	0.6	5.1e3	1.0 \pm 0.5	37	–	120	2.2	6.4e2	0.99	0.075	0.99	EC
B0206	K	0.5	26	1.1 \pm 0.7	5.2	–	0.3f	79	1.1e4	1.4e4	0.024	24	SYN
3C66B	K-A	0.75	3.9	1.0 \pm 0.3	4.0	1.0	0.3f	52	1.9e5	3.6e4	7.7e-3	33	SYN
	K-B	0.60	34	1.2 \pm 0.1	6.2	15.8	0.3f	97	1.2e4	1.9e4	0.024	27	SYN
For A	L	0.9	1.6e4	0.7 \pm 0.3	100	–	450	1.5	1.4e3	0.47	0.055	0.78	EC
3C120	K	0.65	9.2	0.5 \pm 0.1	29	<0.7	1.5	15	6.9e5	1.2e4	4.6e-3	23	EC
3C123	HS	0.5	5.2e3	0.6 \pm 0.3	4.6	<3	0.5	170	1.5	1.3e2	0.85	5.1	SSC
3C129	K	0.5f	3.8	1.0f	1.9	–	0.3f	52	9.7e4	1.8e4	0.010	26	SYN
Pic A	HS	0.74	2.0e3	1.1 \pm 0.1	87	104	0.5	180	3.6e2	1.2e4	0.095	23	SYN
	L-W	0.72	1.3e4	0.6 \pm 0.3	56	–	90	3.5	1.9e2	1.3	0.12	1.1	EC
PKS0521	K	0.6	1.5e2	1.3 \pm 0.3	14	45	0.3f	120	1.7e3	1.2e4	0.050	23	SYN
PKS0637	K	0.8	48	0.9 \pm 0.1	6.2	0.2	0.3f	80	6.0e2	1.6e3	0.077	12	EC
3C179	K-A	0.8	73	1.0f	0.40	<0.06	0.3f	97	15	61	0.34	4.0	EC
	K-B	0.8	1.1e2	1.0f	1.1	<0.06	0.3f	110	23	1.4e2	0.29	5.2	EC
	CL	0.8f	2.9e2	1.0f	0.24	<2.8	2.0	28	3.0	1.1	0.64	1.0	EC
B2 0738	K-A	0.5f	1.7	0.5 \pm 0.4	0.30	–	0.3f	30	4.5e3	4.1e2	0.035	7.4	EC
	HS-B1	0.5f	2.2	1.0 \pm 0.3	0.33	–	0.3f	33	3.4e3	4.0e2	0.039	7.4	SYN
	HS-B2	0.5f	4.0	1.4 \pm 0.5	0.10	–	0.3f	39	4.2e2	89	0.090	4.5	SYN
B2 0755	K	0.5f	54	1.1 \pm 0.2	9.7	–	0.3f	94	6.3e3	1.6e4	0.030	25	SYN
3C207	K	0.8	2.3e2	0.2 \pm 0.3	4.6	–	0.3f	130	46	5.1e2	0.22	8.0	SSC
	HS	0.8	1.6e2	0.7 \pm 1.0	1.3	–	0.3f	110	23	1.7e2	0.29	5.6	SSC
	L	0.9	2.5e2	0.5 \pm 0.4	4.5	–	5.0	12	1.4e2	7.0	0.14	1.9	EC
3C212	HS-S?	0.5f	13	1.0f	0.80	–	0.3f	64	3.1e2	2.3e2	0.10	6.1	SYN
	HS-N?	0.5f	74	1.0f	0.48	–	0.3f	106	14	58	0.35	3.9	SYN
3C219	L	0.8	2.2e3	0.7 \pm 0.2	30	–	50	2.7	4.0e2	1.6	0.091	1.2	EC
4C73.08	L-E	0.85	2.7e2	0.7 \pm 0.4	54	–	180	0.58	6.4e4	2.3	0.012	1.3	EC
	L-W	0.85	5.6e2	0.65f	31	–	180	0.71	1.2e4	0.93	0.023	0.98	EC
Q0957	K-B	0.8f	2.2e2	0.9 \pm 0.6	0.37	<0.11	0.3f	170	1.7	18	0.81	2.6	SSC
	K-C	0.8f	1.3e2	0.9 \pm 0.6	0.11	<0.11	0.3f	140	1.1	6.9	0.96	1.9	SSC
3C254	HS-W	0.8f	98	1.0 \pm 0.8	0.52	–	0.3f	100	15	81	0.34	4.3	SYN
PKS1127	K-A	1.2	1.3	0.5f	1.1	–	0.3f	35	1.1e4	8.6e2	0.024	9.5	EC
	K-B	0.82	16	0.5f	0.89	<0.18	0.3f	72	2.2e2	2.0e2	0.11	5.8	EC
	K-C	0.86	17	0.5f	0.60	<0.15	0.3f	73	1.3e2	1.3e2	0.14	5.1	EC
PKS1136	K-A	0.8f	1.0	1.0f	1.41	0.23	0.3f	25	5.4e4	2.9e3	0.013	14	EC
	K-B	0.8f	41	1.0f	3.7	0.24	0.3f	73	5.4e2	1.2e3	0.081	11	EC
	K-C	0.8f	1.9e2	1.0f	<0.62	0.13	0.3f	110	<9.1	<92	>0.41	< 4.5	EC
3C263	HS-K	0.8f	5.7e2	1.0 \pm 0.1	1.0	0.8	0.3f	160	2.7	72	0.67	4.2	SSC
	HS-B	0.8f	22	1.0f	<0.06	–	0.3f	64	<19	<22	> 0.31	<2.8	SSC
	L-NW	0.8f	1.9e2	0.4 \pm 0.2	0.8	–	8	7.1	51	0.73	0.21	0.90	EC
	L-SW	0.8f	44	0.4 \pm 0.2	0.5	–	8	4.7	2.8e2	0.95	0.10	0.98	EC
4C49.22	K-A	0.8f	56	1.0f	3.9	0.63	0.3f	75	5.9e2	1.7e3	0.08	12	EC
	K-B	0.8f	36	1.0f	1.3	0.02	0.3f	66	3.8e2	7.0e2	0.09	8.9	EC
	K-C	0.8f	74	1.0f	0.99	0.08	0.3f	81	98	3.7e2	0.16	7.2	EC
M84	K-2.5	0.65	3.5	0.8 \pm 0.3	0.63	<30	0.3f	88	1.0e5	1.7e4	9.9e-3	26	SYN
	K-3.3	0.65	13	0.8 \pm 0.3	1.16	<30	0.3f	130	2.6e4	1.6e4	0.02	25	SYN
3C273	K-A1	0.65	20	0.6 \pm 0.1	38.1	5.2	0.3f	56	4.8e4	4.8e4	0.01	36	SYN
	K-B1	0.65	2.2e2	0.9 \pm 0.1	23.2	5.2	0.3f	110	8.1e2	8.7e3	0.069	21	EC
	K-D/H3	0.65	3.2e2	0.8 \pm 0.1	8.27	8.2	0.3f	120	1.6e2	2.6e3	0.13	14	EC
M87	K-HST1	0.7	77	1.3 \pm 0.1	81.9	20	0.3f	220	1.3e5	4.8e5	9.0e-3	78	SYN
	K-A	0.7	3.5e2	1.3 \pm 0.2	67.8	100	0.3f	330	1.1e4	1.9e5	0.024	57	SYN
	K-D	0.7	2.6e3	1.6 \pm 0.1	142	1000	0.3f	590	1.2e3	1.4e5	0.059	52	SYN
3C280	HS-W	0.8	7.2e2	1.3 \pm 1.0	0.79	0.99	0.3f	200	0.95	32	1.0	3.2	SSC
	HS-E	0.8	3.3e2	1.2	0.34	0.23	0.3f	160	1.3	21	0.90	2.7	SSC

TABLE 2—*Continued*

name	comp	α_R	f_R [mJy]	α_X	f_X [nJy]	f_O [μ Jy]	θ [$''$]	$B_{eq}(1)$ [μ G]	$R_{SSC}(1)$	$R_{EC}(1)$	δ_{SSC}	δ_{EC}	class	
Cen A	K-NX1	0.8f	36	1.5	5.8	—	0.3f	270	6.3e4	1.1e5	0.01	48	SYN	
	K-AX1	0.8f	5.2e2	1.5	110	—	0.3f	580	2.2e4	5.4e5	0.02	81	SYN	
	K-AX2	0.8f	4.8e2	1.5	14	—	0.3f	570	3.1e3	7.1e4	0.04	41	SYN	
	K-AX3	0.8f	7.4e2	1.2	28	—	0.3f	640	3.3e3	1.1e5	0.04	49	SYN	
	K-AX4	0.8f	3.3e2	1.2	14	—	0.3f	510	5.5e3	8.6e4	0.03	44	SYN	
	K-AX6	0.8f	71	1.2	23	—	0.3f	330	9.0e4	3.0e5	0.01	67	SYN	
	K-BX2	0.8f	88	1.0	66	—	0.3f	350	1.9e5	7.8e5	7.8e-3	92	SYN	
Cen B 4C19.44	K-BX5	0.8f	7.5e2	1.0	50	—	0.3f	640	5.7e3	2.0e5	0.03	59	SYN	
	L	0.78	3.7e4	0.9 \pm 0.2	220	—	180	3.5	3.8e2	1.9	0.09	1.2	EC	
	K-A	0.8f	57	1.0f	8.3	0.3	0.3f	86	5.6e2	1.7e3	0.08	12	EC	
	K-B	0.8f	23	1.0f	0.24	0.04	0.3f	66	63	79	0.19	4.3	EC	
	K-C	0.8f	13	1.0f	0.37	<0.06	0.3f	56	2.3e2	1.6e2	0.11	5.4	EC	
	K-D	0.8f	16	1.0f	0.25	<0.06	0.3f	60	1.1e2	98	0.15	4.6	EC	
	K-E	0.8f	6	1.0f	0.25	<0.06	0.3f	45	4.9e2	1.6e2	0.08	5.4	EC	
	K-F	0.8f	12	1.0f	0.70	<0.06	0.3f	55	4.9e2	3.2e2	0.08	6.8	EC	
	K-G	0.8f	13	1.0f	0.62	<0.06	0.3f	56	3.8e2	2.7e2	0.09	6.5	EC	
	K-H	0.8f	>1	1.0f	0.41	<0.06	0.3f	>27	>1.2e4	>6.4e2	>0.02	< 8.6	EC	
	K-I	0.8f	87	1.0f	0.66	—	0.3f	97	24	1.1e2	0.28	4.8	EC	
	3C295	HS-NW	0.65	1.3e3	0.9 \pm 0.5	3.9	0.078	0.3f	190	4.4	2.7e2	0.55	6.5	SSC
		HS-SE	0.65	6.3e2	0.9 \pm 0.5	1.1	<0.02	0.3f	150	3.6	1.1e2	0.60	4.8	SSC
		L	0.9	6.5e3	0.4 \pm 0.2	3.4	—	1.5	75	0.76	9.4	1.1	2.1	SSC
	3C303	HS	0.84	2.6e2	0.4 \pm 0.2	4.0	7.5	1.0	42	2.2e2	2.5e2	0.12	6.3	SSC
GB1508	K	>0.8	0.43	0.9 \pm 0.4	1.1	<0.2	0.6	32	1.6e4	81	0.02	4.3	EC	
3C330	HS-NE	1.0	1.3e3	0.5f	0.34	<0.5	0.3f	200	0.32	19	1.6	2.7	SSC	
	HS-SW	1.0	1.3e2	0.5f	0.09	<0.5	0.3f	100	2.6	16	0.68	2.5	SSC	
	L-NE	0.9	2.6e2	0.5f	0.28	—	3.5	15	8.9	0.90	0.42	1.0	EC	
	L-SW	1.0	2.3e2	0.5f	0.32	—	3.5	15	12	1.1	0.37	1.0	EC	
NGC6251	K	0.64	2.2e2	0.2 \pm 0.4	2.3	—	10	7.9	1.4e3	13	0.06	2.4	EC	
3C351	HS-J	0.7	1.9e2	0.5 \pm 0.1	4.3	2.5	0.3f	110	1.0e2	9.2e2	0.16	9.7	SSC	
	HS-L	0.7	4.5e2	0.9 \pm 0.1	3.4	3.8	0.8	59	36	1.1e2	0.24	4.8	SSC	
	HS-A	0.8	4.5	0.9f	<0.05	—	0.3f	37	<3.0e2	<69	> 0.10	<4.1	SSC	
	L-N	1.0	72	0.6 \pm 0.8	1.1	—	10	4.0	5.9e2	2.0	0.08	1.3	EC	
	L-S	0.9	73	0.6 \pm 0.8	0.7	—	10	4.0	3.7e2	1.3	0.09	1.1	EC	
3C371	K-A	0.76	37	1.0f	6.7	5.8	0.3f	81	6.9e3	1.2e4	0.03	23	SYN	
	K-B	0.73	15	0.7 \pm 0.3	16	3.4	0.3f	62	6.4e4	4.6e4	0.01	36	SYN	
3C390.3	HS-NE-B	0.7	3.5e2	0.9 \pm 0.1	4.5	1.8	1.1	49	2.9e2	3.6e2	0.10	7.1	SYN	
	HS-SW	0.7	67	0.4 \pm 0.2	3.5	—	10	4.7	8.1e3	23	0.03	2.9	EC	
Cyg A	HS-A	0.55	4.0e4	0.8 \pm 0.2	19	—	1.2	180	1.0	1.3e2	0.98	5.0	SSC	
	HS-D	0.50	5.0e4	0.8 \pm 0.2	29	<8	1.2	190	1.2	1.7e2	0.94	5.5	SSC	
3C452	L	0.78	4.0e3	0.7 \pm 0.3	41	—	80	2.4	4.7e2	1.3	0.09	1.1	EC	

NOTE.—*Observables* – α_R : radio spectral index at 5 GHz, f_R : radio flux density at 5 GHz in mJy, α_X : X-ray spectral index at 1 keV, f_X : X-ray flux density at 1 keV in nJy, f_O : optical flux density at 5×10^{14} Hz in μ Jy, and θ : radial size of the emitting region in arcsec. Parameters with suffix f is assumed to be a listed value. *Model results* – $B_{eq}(1)$: the equipartition magnetic field for no beaming $\delta = 1$, $R_{SSC}(1)$: the ratio of observed X-ray flux density to that expected from SSC model for $\delta = 1$, $R_{EC}(1)$: the ratio of observed X-ray flux density to that expected from EC model for $\delta = 1$, δ_{SSC} : the Doppler beaming factor required to hold equipartition i.e., $R_{SSC}(\delta_{SSC}) \simeq 1$, and δ_{EC} : the Doppler beaming factor required to hold equipartition for EC model, i.e., $R_{EC}(\delta_{EC}) \simeq 1$. class: Most likely scenario of producing observed X-rays.